

https://dspace.org/

The Design and Development of a DexamethasoneTranfersome PF127HA StimuliResponsive Hydrogel for IntraArticular Therapy in Osteoarthritis

Atang Motaung; T Rants'o; R Badhe; Khonzisizwe Somandi; Yahya Choonara

https://hdl.handle.net/10539/48492
DOAJ

Downloaded from a DSpace repository. https://dspace.org/

Nano Select

RESEARCH ARTICLE OPEN ACCESS

The Design and Development of a Dexamethasone-Tranfersome-PF-127/HA Stimuli-Responsive Hydrogel for Intra-Articular Therapy in Osteoarthritis

Atang Motaung[1] | Thankhoe A. Rants'o[2] | Ravindra V. Badhe[3] | Khonzisizwe Somandi[1] | Yahya E. Choonara[1]

[1]Wits Advanced Drug Delivery Platform Research Unit, Department of Pharmacy and Pharmacology, Faculty of Health Sciences, School of Therapeutic Science, University of Witwatersrand, Johannesburg, South Africa | [2]Department of Pharmacology and Toxicology, College of Pharmacy, University of Utah, Salt Lake City, Utah, USA | [3]Pharmaceutical Chemistry Department, Marathwada Mitra Mandal's College of Pharmacy, Pune, India

Correspondence: Yahya E. Choonara (yahya.choonara@wits.ac.za)

Received: 10 April 2025 | **Revised:** 13 June 2025 | **Accepted:** 15 July 2025

Funding: This study was supported by the National Research Foundation (NRF) of South Africa under the SARChI Chair program (Grant No. PPNT230823145247).

Keywords: DEX-loaded transfersomes | hydrogel | interleukin-4 | intra-articular | osteoarthritis

ABSTRACT

Osteoarthritis (OA), a prevalent degenerative joint disease, significantly impairs mobility and quality of life, often necessitating frequent intra-articular (IA) injections to manage pain and inflammation. This study develops and characterizes a dexamethasone (DEX)-loaded transfersome-based hydrogel (DEX-tNPs-PF127/HA) for IA delivery in OA treatment. The formulation is optimized to enable controlled drug release and improved stability, aiming to reduce IA injection frequency while maintaining therapeutic efficacy. DEX-loaded transfersomes (tNPs) are synthesized via thin-film hydration and incorporated into a thermoresponsive hydrogel composed of Pluronic F-127 (PF-127) and hyaluronic acid (HA). Morphological evaluation, particle size analysis, zeta potential measurements, encapsulation efficiency assessment, and rheological characterizations are conducted. DEX-tNPs exhibit a nanoscale size (~76 nm), with a high encapsulation efficiency (98%) and a cationic surface charge. In vitro drug release studies demonstrate sustained DEX release over 6 weeks under physiological conditions. Biocompatibility, determined using RAW 264.7 macrophages, reveals cell viability above 70%. Interleuken-4 (IL-4) quantification indicates an initial immunomodulatory effect from the blank-tNPs hydrogel, with a slight reduction upon DEX encapsulation. The hydrogel exhibits favorable shear-thinning and self-healing properties, facilitating smooth IA injection. These findings highlight the DEX-tNPs-PF127/HA hydrogel as a promising candidate for sustained IA therapy in OA. Further in vivo studies are warranted.

1 | Introduction

Osteoarthritis (OA) is a chronic, degenerative joint disease that affects over 7% of the global population, placing a considerable burden on individuals and healthcare systems worldwide [1]. OA is a heterogeneous disease characterized by the progressive degeneration of articular cartilage, subchondral bone remodeling, and chronic synovial inflammation, primarily affecting weight-bearing joints such as the knees, hips, and spine [2].

The molecular pathophysiology of OA involves a complex interplay between mechanical stress and immune dysregulation.

This is an open access article under the terms of the Creative Commons Attribution License, which permits use, distribution and reproduction in any medium, provided the original work is properly cited.

© 2025 The Author(s). *Nano Select* published by Wiley-VCH GmbH.

Pro-inflammatory cytokines such as interleukin-1β (IL-1β), tumor necrosis factor-α (TNF-α), and interleukin-6 (IL-6) promote the expression of matrix metalloproteinases (MMPs) and a disintegrin and metalloproteinase with thrombospondin motifs, leading to extracellular matrix degradation [3]. Conversely, anti-inflammatory cytokines like IL-4 and IL-10 downregulate MMPs and promote M2 macrophage polarization, thereby aiding cartilage preservation [4].

Current treatment is primarily palliative, involving analgesics (e.g., acetaminophen), non-steroidal anti-inflammatory drugs, and IA medications such as corticosteroids and hyaluronic acid (HA). However, systemic drug administration has low joint bioavailability, reducing efficacy and increasing side effects [5]. Meanwhile, transdermal delivery aids superficial inflammation but struggles to reach deep tissues, limiting effectiveness [6]. Notably, OA joints have lower HA levels, reducing lubrication and increasing pain. IA HA and corticosteroids offer site-specific therapy with reduced systemic side effects but face rapid clearance, necessitating frequent, and costly injections. Innovative strategies are needed to prolong drug retention and enhance therapeutic benefits [7].

To address these limitations, nanotechnology has been explored to improve IA drug retention, stability, and sustained release. Nanoparticles (NPs) can enhance the residence time of therapeutic agents in the joint space and protect them from enzymatic degradation [8]. Concurrently, hydrogels-three-dimensional hydrophilic networks-mimic the native extracellular matrix, provide lubrication, and reduce joint friction. The combination of NPs and hydrogels in hybrid drug delivery systems has shown synergistic potential for OA therapy by enabling controlled, localized, and prolonged drug release [9, 10].

Recent studies have demonstrated that such NP-loaded hydrogels can effectively modulate the OA microenvironment, extend drug retention, and improve therapeutic outcomes in preclinical models [11–13]. Among responsive hydrogel systems, thermoresponsive hydrogels are particularly attractive for IA applications due to their sol–gel transition at physiological temperatures, allowing minimally invasive administration and in situ gelation [14]. PF-127, a biocompatible triblock copolymer of poly (ethylene oxide)–poly (propylene oxide)–poly (ethylene oxide) (PEO100–PPO65–PEO100), is readily water soluble at low temperatures and has the ability to form gels at temperatures close to body temperature [15]. PF-127 has been widely used in controlled drug release systems mainly because of its low immunogenicity and toxicity. However, its clinical performance is hampered by poor mechanical integrity and rapid drug release. These shortcomings can be mitigated by incorporating complementary polymers such as HA and chitosan, which enhance mechanical strength, gel stability, and bioadhesion [13, 16].

In line with recent advances in stimuli-responsive delivery systems, such as the NIR-triggered nanoplatform developed by Rybak et al. for on-demand wound treatment, there is growing interest in smart biomaterials that enable site-specific, controlled drug release [17].

Building on this, our study aimed to address the shortcomings of current OA treatments. We developed a novel stimuli-responsive IA delivery platform by integrating dexamethasone (DEX)-loaded lipid-based nanocarriers (tNPs) into a PF-127/HA hydrogel matrix. This system was designed to exploit the thermosensitive properties of PF-127 and the joint-targeting benefits of high molecular weight HA for site-specific, sustained drug delivery in OA treatment.

2 | Materials and Methods

2.1 | Molecular Modeling of the DEX-tNP Complex

Using the Maestro Materials Science platform of Schrödinger software (version 2023-2), the molecular interactions of DEX and the tNPs were assessed [18]. Mimicking the in vitro study, a tNP was computationally designed from four components, including phosphatidylcholine, cholesterol, polysorbate 80, and dimethyl dioctadecyl ammonium bromide (DDAB). The 3D chemical structures of the first three components were obtained from Mol-Instincts database (Mol-Instincts IDs: CT1089733823, CT1001897301, and CT1080213202, respectively) while that of DDAB was downloaded from PubChem [18, 19]. These were all treated as monomers and subjected to the Polymer Builder tool to form a polymer. In the Polymer Builder, the co-polymeric system was randomized in a 1:1 ratio of the monomers, and the system was minimized under the OPLS4 force field. Lastly, the system was optimized for Desmond calculations and allowed to form an amorphous cell at a density of 0.5 g/cm^3 [19]. Next, the final polymer was modeled under the Nanoparticle Builder as a sphere to generate a tNP [20]. However, to form a drug-loaded tNP and simulate associated interactions, the resulting tNP was submitted to the Disordered System Builder and ran for simulation with DEX as a substrate. The disorder options included having the DEX-tNP in an SPC buffered water model that mimicked the physiological environment by adding sodium and chloride ions to a concentration of 0.15 M. The final tNP was then assessed for successful drug loading and drug–tNP intermolecular interactions [19, 21].

2.2 | Materials

Phosphatidylcholine, cholesterol, DDAB, polysorbate 80, PF-127, DEX, HA (MW: 850 kDa), bovine serum albumin (BSA), Dulbecco's Modified Eagle's Medium (DMEM), fetal bovine serum (FBS), penicillin and streptomycin and phosphate-buffered saline (PBS, pH 7.4), 3-(4,5-dimethyl-2-thiazolyl)-2,5-diphenyltetrazolium bromide (MTT reagent), solubilizing agent (acid-isopropanol, 0.04 N HCl in isopropanol), and high-performance liquid chromatography (HPLC)-grade methanol and chloroform.

2.3 | Methods: Preparation of tNPs by Thin Film Hydration

The lipid phase, consisting of phosphatidylcholine, polysorbate 80, cholesterol, and DDAB, was dissolved in chloroform and methanol, then evaporated at 60°C to form a thin film in a round-bottomed flask. After overnight residual solvent removal in a

26884011, 2025, 12, Downloaded from https://onlinelibrary.wiley.com/doi/10.1002/nano.70047 by University Of Witwatersrand, Wiley Online Library on [15/12/2025]. See the Terms and Conditions (https://onlinelibrary.wiley.com/terms-and-conditions) on Wiley Online Library for rules of use; OA articles are governed by the applicable Creative Commons License

fume hood, the film was hydrated with a DEX solution (10 mg in 10 mL deionized water), forming vesicles. The suspension was sonicated using a probe sonicator (Sonics Vibra cell, Newtown, CT, USA) on ice for 10 min at 40% amplitude to homogenize the tNPs [22]. Synthesis of the blank-tNPs followed the same process without DEX entrapment.

2.3.1 | Determination of Particle Size, Morphology, and Zeta Potential of the tNPs

The size, polydispersity index (PDI), and zeta potential of tNPs were measured using dynamic light scattering (DLS) on a Zeta-Sizer NanoZS (Malvern Instruments (Pty) Ltd., Worcestershire, UK) after sample dilution (1:4) with phosphate-buffered saline (PBS) at pH 7.4 [23]. Measurements were conducted in triplicate in a quartz cuvette to measure the size and PDI, and a folded capillary cell for the zeta potential [23].

Scanning electron microscopy (SEM) (Jeol JSM-120, Tokyo, Japan) analyzed morphology of the tNPs after drying and gold-palladium coating on an aluminum stub. For transmission electron microscopy (TEM), a diluted suspension of tNPs was dropped onto a carbon-coated copper grid. A 2% (v/v) uranyl acetate negative stain solution was added to the 3 mM forman-coated copper grid of 300 mesh for 90 s and allowed to dry overnight to be visualized using the TEM (FEI Tecnai T12, FEI Company, Hillsboro, OR, USA) [23].

2.3.2 | Drug Entrapment Efficiency

The indirect method determined %EE by separating free drug from drug-loaded vesicles using Amicon Ultra4 filter tubes-Millipore Corp., USA (10 kDa MWCO). A 2 mL suspension ($n = 3$) was centrifuged at 2500 rpm for 45 min. The supernatant's drug content was analyzed via UV–vis at 245 nm to calculate %EE using Equation (1) below [24]:

$$\mathrm{EE} = \frac{\text{Total amount of the drug added} - \text{Amount of the free drug}}{\text{Total amount of the drug added}} \times 100 \quad (1)$$

2.3.3 | Degree of Deformability

Deformability was assessed by extruding the tNPs through a 0.1 μm polycarbonate filter membrane (Sigma Chemicals, UK) and measuring size via DLS. The deformability index was then calculated using the Equation (2) below:

$$\mathrm{D} = J \times \left(\frac{Rv}{Rp}\right) \quad (2)$$

where D is the deformability index, J is the amount of sample extruded, Rv is the vesicle size after extrusion, and Rp is the filter pore size.

2.3.4 | Physicochemical Characterizations of tNPs

2.3.4.1 | Thermogravimetric Analysis. Freshly synthesized tNPs were frozen and lyophilized [25]. To evaluate the thermal degradation properties of the DEX, blank-tNPs, and DEX-loaded tNPs, the thermal degradation of DEX, blank-tNPs, and DEX-loaded tNPs were analyzed using thermogravimetric analysis (TGA) (PerkinElmer, TGA 4000, Llantrisant, Wales, UK) [26]. Samples (~15 mg) were heated from 30°C to 900°C at 10°C/min increments and further held for a minute at 900°C.

2.3.4.2 | X-Ray Diffraction. X-ray diffraction (XRD) analysis was conducted on DEX, blank-tNPs, and DEX-loaded tNPs using a powder x-ray diffractometer (PANalytical 3 kW X'pert Powder, Cambridge, UK). Samples were scanned from 2 to 60 h using Cu-Kα radiation (2Θ/min) at 40 kV, 30 mA, and a 5°C/min temperature ramp.

2.3.4.3 | Fourier Transform Infrared Spectroscopy. Fourier transform infrared (FTIR) spectroscopy was performed using the Perkin Elmer Spectrum 2000 ATR-FTIR spectrometer fitted with a single reflection (PerkinElmer 100, Llantrisant, Wales, UK). Similar quantities of the DEX, blank-tNPs, and DEX-loaded tNPs were placed on the diamond stage, and analysis was performed within a range of 650–4000 cm^{-1}.

2.3.5 | Determination of the Physical Stability of DEX-Loaded tNPs

DEX-loaded tNPs were stored at 4°C (mimicking long-term storage conditions) and 25°C (mimicking short-term storage conditions) for 3 months. Stability was assessed by measuring size, PDI, zeta potential, turbidity, and visual changes.

2.3.6 | In Vitro Drug Release

A cellulose dialysis membrane was prepared according to the manufacturer's manual instructions. The DEX-loaded tNPs, blank-tNPs, and free DEX were transferred into respective dialysis tubes and placed in receivers with PBS (pH 7.4) as the release media. The receivers were placed into a gently shaking (20–25 rpm) incubator at 37°C. Samples were withdrawn from the receivers at intervals (0.5, 1, 2, 4, 6, 8, 10, 12, 24, 48, and 72 h) and immediately replaced with the same amount of fresh buffer, pre-equilibrated at 37°C. The samples ($n = 3$) were assayed using UV–vis at 245 nm [27].

2.3.7 | HA/PF-127 Hydrogel Synthesis and tNP Loading in HA/PF-127 Hydrogel

Using the cold method, PF-127 was added into deionized water while stirring at a constant temperature of 4°C to form 17% of PF-127 (w/v) [28]. HA was added to the PF-127 solution to form 1% (w/v) and stored overnight at 4°C until a clear solution was obtained to fully hydrate the polymers [28, 29]. Finally, a suspension of the tNPs was added to the PF-127/HA hydrogel and mixed to form a homogenous mixture. Physico-

26884011, 2025, 12, Downloaded from https://onlinelibrary.wiley.com/doi/10.1002/nano.70047 by University Of Witwatersrand, Wiley Online Library on [15/12/2025]. See the Terms and Conditions (https://onlinelibrary.wiley.com/terms-and-conditions) on Wiley Online Library for rules of use; OA articles are governed by the applicable Creative Commons License

chemical characterizations were performed for hydrogels loaded with DEX-loaded tNPs, hydrogels containing blank tNPs, and non-loaded hydrogels, as detailed in Section 2.2.5.

2.3.8 | Brunauer–Emmett–Teller Analysis for Hydrogel Pore Analysis

The composite's surface area was measured using the Brunauer–Emmett–Teller (BET) surface adsorption method, with freeze-dried samples, loaded in a glass tube, de-gassed, and immersed in liquid nitrogen (adsorbate) for analysis.

2.3.9 | Determination of the Gelation Time of DEX-tNPs-PF-127/HA Hydrogel

Aliquots of the composite were put in glass vials and placed into a water bath at 37°C to determine the gelation time. After set time intervals of 30 s, the vials were inverted to determine the gelation time and to verify the sol–gel transition [30, 31].

2.3.10 | Syringeability of DEX-tNPs-PF-127/HA Hydrogel

Syringeability was measured using a TA-XT Plus texture analyzer (Stable Micro Systems, Surrey, UK) in compression mode at room temperature. A 1 mL hydrogel sample was extruded through a 22-gauge needle at 1 mm/s, and the maximum force was analyzed from the texture analysis profile [30].

2.3.11 | In Vitro Drug Release Using a Knee Joint Simulator

The constructed knee simulator (Figure S1), based on Indian Design Registration 375583-001, mimics joint movement per ISO 14243 and ASTM F1223. Made of HDPE and polyacrylic, it operates at 1 Hz, allows 45° flexion on both sides, accommodates synovial fluid-like media, and maintains 37°C for drug formulation testing. Artificial synovial fluid with BSA, phosphatidylcholine, and HA in PBS (pH 7.4) was used as a release medium in a knee joint simulator, where tNPs and hydrogel systems were injected and mixed. Samples were withdrawn at 0.5, 1, 2, and 4 h, and replaced with fresh artificial synovial fluid-like medium equilibrated at 37°C. Samples were evaluated using UV–vis at a wavelength of 245 nm to determine drug release kinetics.

2.3.12 | Rheological Characterization of the DEX-tNPs-PF-127/HA Hydrogel

An AR 2000 Rheometer (TA instruments, USA) was used to evaluate temperature ramp, stress sweep, frequency sweep, yield stress, and thixotropy tests of HA/PF-127 hydrogel as well as the hydrogel composite. Stress and frequency sweep tests were performed at 37°C to determine the linear viscoelastic (LVE) region. The storage modulus (G') and loss modulus (G'') were analyzed to assess elasticity and viscosity, respectively.

2.3.13 | Cytocompatibility Studies

2.3.13.1 | Cell Culture. The 264.7 RAW macrophage cells were cultured in Dulbecco's Modified Eagle Medium (DMEM) supplemented with 10% (v/v) fetal bovine serum (FBS) and 1% (v/v) antibiotics (penicillin and streptomycin). The cells were incubated in a 95% humidified incubator (NUAIRE, Radobio, China) at 37 °C with 5% CO_2. The culture medium was refreshed daily until the cell confluency reached ≈90%.

2.3.13.2 | Cell Viability and Proliferation Assay of 264.7 RAW Macrophage Cells. The effects of DEX, Blank-tNPs, DEX-tNPs, Blank-tNPs hydrogel, and DEX-tNP hydrogel composites on RAW 264.7 macrophage cell viability were analyzed using the Cell Proliferation Kit I assay (Roche, Basel, Switzerland). Cells were seeded in 96-well plates (5×10^3 cells/well), incubated at 37°C, 5% CO_2 for 24 h, then treated with test formulations at varying concentrations (50, 25, 12.5, and 6.25 μg/mL). DMSO (4% v/v) was the negative control, and untreated cells served as the positive control. After 48 h treatment, the MTT solution was added for 4 h, at 37 °C and 5% CO_2, and formazan crystals were dissolved using 100 μL of the solubilizing agent (acid-isopropanol, 0.04 N HCl in isopropanol). Absorbance was measured at 595 nm using a TECAN GENios (TECAN Group Ltd., Männedorf, Switzerland, serial no. 12900400226) to determine cell viability using Equation (3).

$$\text{Cell viability} = \frac{\text{A treatment} - \text{Aneg. control}}{\text{Apos. control} - \text{Aneg. control}} \times 100 \ (\text{where}, A = \text{absorbance}) \quad (3)$$

2.3.13.3 | IL-4 Quantification From RAW 264.7 Macrophage Cells After Various Treatments. RAW 264.7 macrophage cells (5×10^4 cells/well) were seeded in a 96-well plate and incubated for 24 h for adherence. Cells were then treated in triplicate with 50 μg/mL of DEX, Blank-tNPs, DEX-tNPs, Blank-tNPs hydrogel, or DEX-tNPs hydrogel composites for another 24 h. After treatment, 50 μL of cell culture supernatant was collected and added to an ELISA plate, incubated at room temperature for 3 h, washed with 400 μL of wash buffer (PBS, 1% Tween-20) for 15 s cycles, and reacted with 3,3',5,5'-Tetramethylbenzidine substrate (100 μL) for 10 min, at room temperature while avoiding direct light. The stop solution (1 M phosphoric acid) at 100 μL was added, with the development of a strong dark blue color. Absorbance was then measured at 450 nm (primary) and 620 nm (reference) using a microplate reader.

3 | Results

3.1 | In Silico Analysis of the DEX-tNPs Complex

Modeling of the DEX-tNPs complex in the physiological solvent system (Figure 1a) showed successful DEX loading in the centroid of the tNPs (Figure 1b). DEX-tNP interactions revealed that DEX mainly interacted with phosphatidylcholine through nonpolar interactions and at least with one hydrogen bond (Figure 1c). This indicated a balanced interaction ideal for controlled drug release [19].

26884011, 2025, 12, Downloaded from https://onlinelibrary.wiley.com/doi/10.1002/nano.70047 by University Of Witwatersrand, Wiley Online Library on [15/12/2025]. See the Terms and Conditions (https://onlinelibrary.wiley.com/terms-and-conditions) on Wiley Online Library for rules of use; OA articles are governed by the applicable Creative Commons License

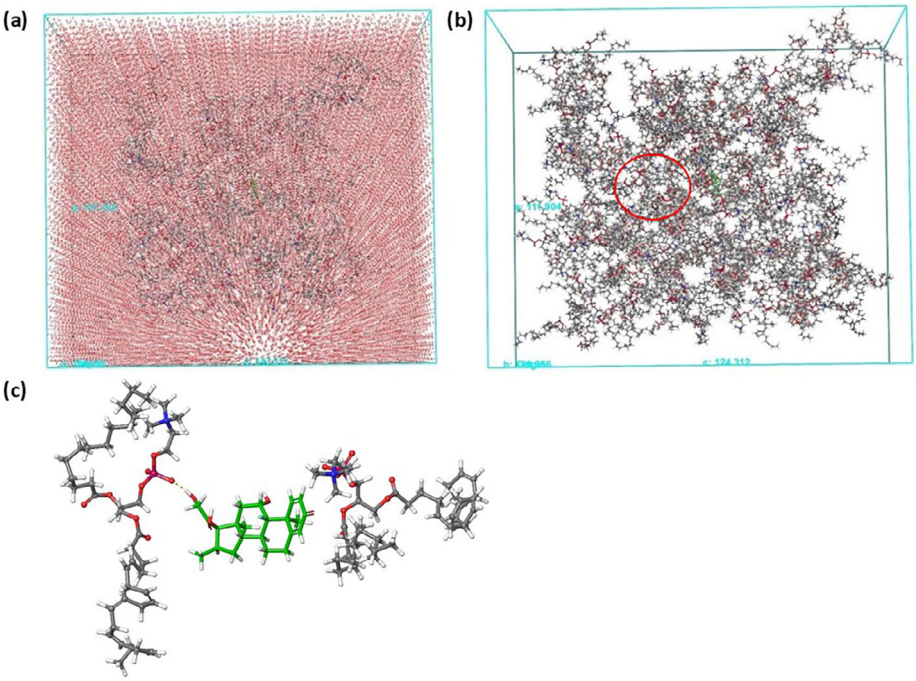

FIGURE 1 | In silico simulation of DEX-tNP complex. (a) The DEX-tNP complex in the buffered water model. (b) The successful DEX-loading in the tNP. (c) The established molecular interactions between DEX and transfersomal constituents (only two monomers closest to DEX selected for visibility).

3.2 | tNP Synthesis and DEX Loading

3.2.1 | Size and Morphology of tNPs and tNPs-PF-127/HA Composite

DLS analysis showed that loading DEX into the tNPs increased the vesicle size from 60.93 to 76.43 nm, decreased the zeta potential from 15.8 to 10.58 mV, and reduced the PDI from 0.191 to 0.183, suggesting successful drug loading into the tNPs (Table S2). The decrease in zeta potential was due to the negatively charged DEX. SEM and TEM analyses showed homogenous dispersion, nanosizes (~79–115 nm), and spherical morphology of tNPs (Figure 2a–d), essential for drug loading/delivery applications, biological barrier permeation, and sustained release.

SEM confirmed the porous structure of the blank and DEX-tNPs-PF-127/HA hydrogels (Figure 3a,b), while BET analysis indicated decreased pore sizes upon DEX-tNPs loading (Table S3).

3.3 | Degree of Deformability of tNPs

After 10 extrusion passes, DEX-loaded tNPs size decreased from 75 to 64 nm, with PDI reduced from 0.183 to 0.134. The vesicles had a degree of deformability of 660 μL and a size reduction of 16% confirming the flexibility of the tNPs.

3.4 | Thermal and Physicochemical Characterization of Formulated tNPs and tNPs-PF-127/HA Composite

Thermograms confirmed DEX encapsulation in the tNPs, showing its thermal degradation, while the blank-tNPs lacked DEX's degradation traits (Figure 4a). Hydrogels exhibited PF-127 and HA degradation, with HA less prominent due to its low concentration (1% w/v), Figure 4b. XRD analysis revealed the crystalline nature of DEX, whereas the loaded tNPs showed broad peaks, indicating an amorphous nature, Figure 4c. The Hydrogels had similar diffractograms, with reduced PF-127 peak intensity (Figure 4d).

The FTIR analysis of DEX, blank-tNPs, and DEX-loaded tNPs was conducted to obtain insights of the encapsulation of the drug into the tNPs. Figure 3a represents the FTIR spectra. FTIR spectra of both the blank and DEX-loaded tNPs showed identical patterns, with signals at 3375.35 cm^{-1} (O–H), 1736.88 cm^{-1} (C═O), 2853.47 and 2923.14 cm^{-1} (CH2), and 1243.65 cm^{-1} (P═O). The absence of DEX-specific bands in the DEX-loaded tNPs spectrum suggests successful encapsulation of DEX (Figure 4e).

The FTIR spectra of the blank-PF-127/HA hydrogel showed the characteristic of PF-127 signals at approximately 2900 cm^{-1} (C–H), 2881 cm^{-1} (O–H), 1373 cm^{-1} (C–O) cm^{-1}, and an HA signal at approximately 1622.22 cm^{-1} belonging to C═O carbonyl stretch [32] (Figure 4f). The absence of tNPs signals (see Figure 4f) in the DEX-loaded hydrogel spectrum indicated successful encapsulation of DEX-loaded tNPs within the hydrogel matrix, confirming the drug incorporation. The PF-127/HA hydrogels were formed potentially through hydrogen-bonding interactions between hydroxyl (–OH) groups of the PF-127 and the carboxyl groups or hydroxyl groups of the HA (Figure 4g).

3.5 | Physical Stability of DEX-Loaded tNPs

Physical stability studies over 3 months showed minimal changes in size, with a slight reduction in zeta potential and an increase

26884011, 2025, 12, Downloaded from https://onlinelibrary.wiley.com/doi/10.1002/nano.70047 by University Of Witwatersrand, Wiley Online Library on [15/12/2025]. See the Terms and Conditions (https://onlinelibrary.wiley.com/terms-and-conditions) on Wiley Online Library for rules of use; OA articles are governed by the applicable Creative Commons License

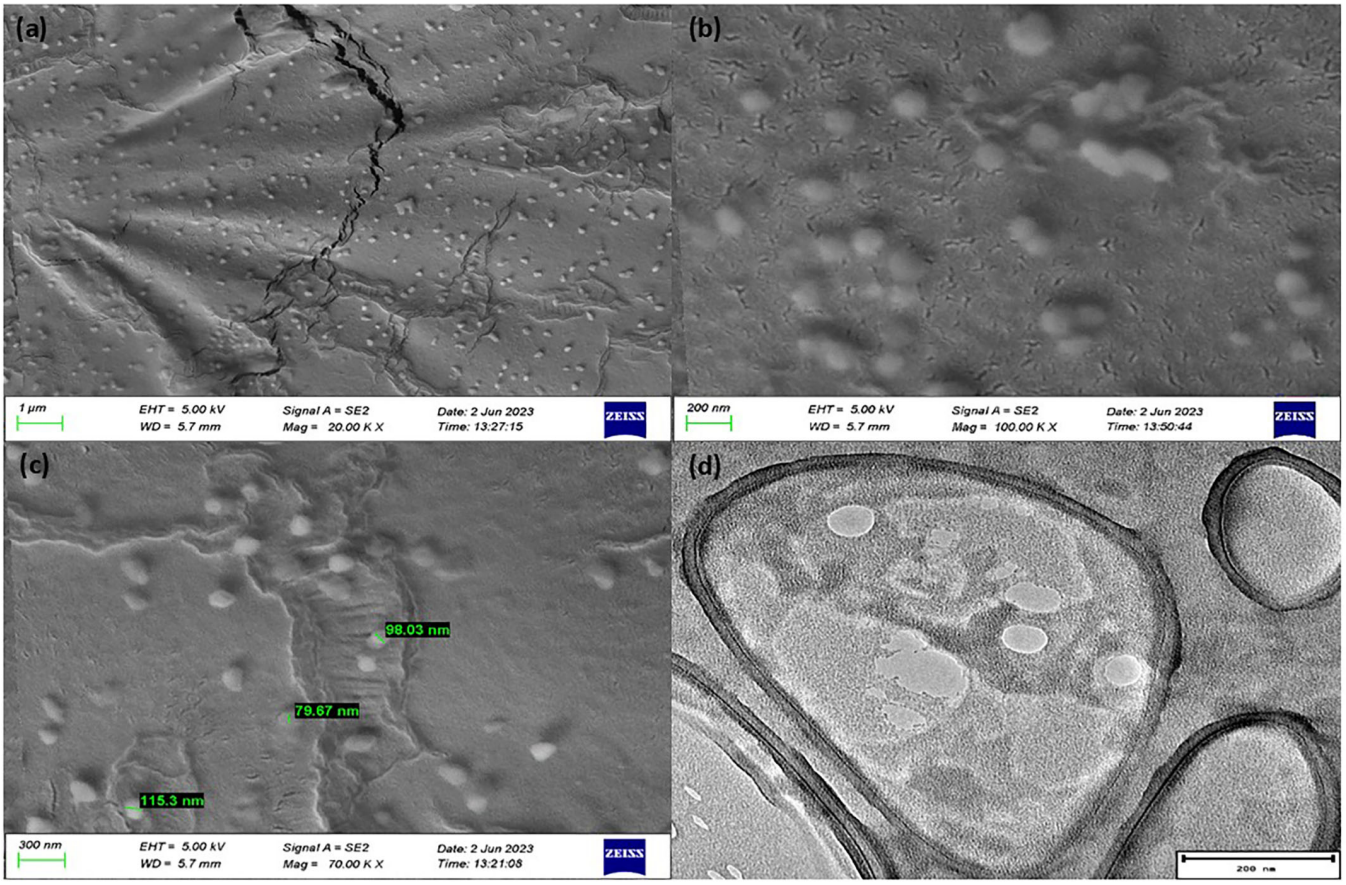

FIGURE 2 | Morphology of the tNPs shown by SEM at a scale of 1 µm, showing overall size and morphology (a), SEM image of tNPs at 200 nm (b), and an annotated SEM image of tNPs showing particle size at 200 nm (c). TEM imagery of the tNPs at a scale of 200 nm (d).

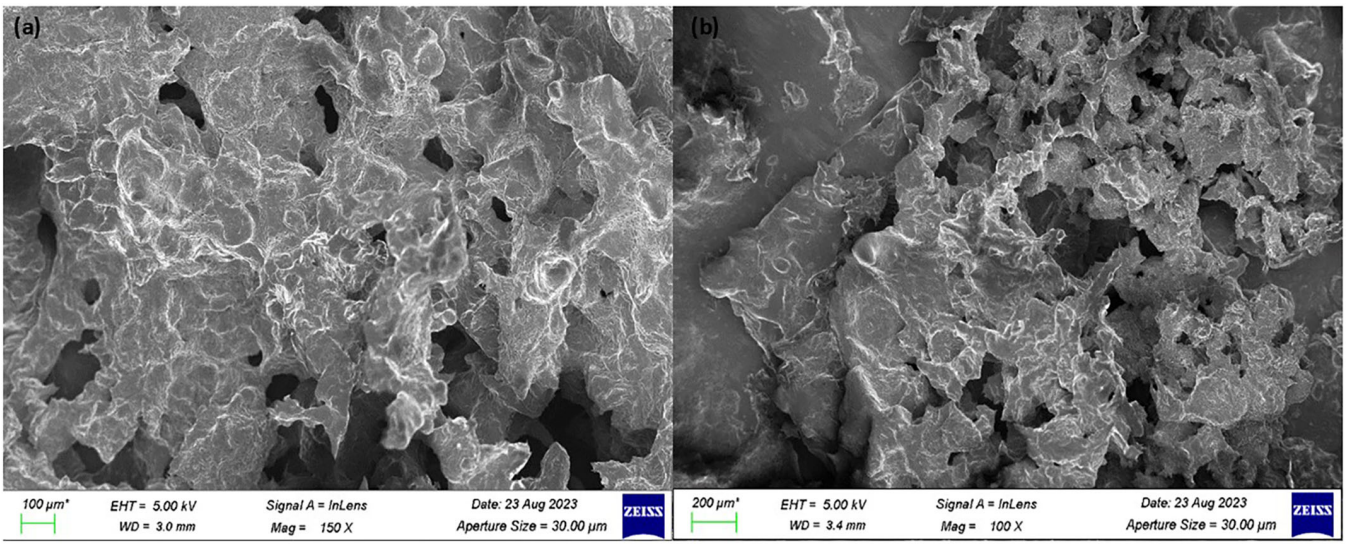

FIGURE 3 | SEM images of (a) blank-tNPs-PF-127/HA hydrogel and (b) DEX-tNPs-PF-127/HA hydrogel, illustrating the porous microstructure of the hydrogel matrix.

26884011, 2025, 12, Downloaded from https://onlinelibrary.wiley.com/doi/10.1002/nano.70047 by University Of Witwatersrand, Wiley Online Library on [15/12/2025]. See the Terms and Conditions (https://onlinelibrary.wiley.com/terms-and-conditions) on Wiley Online Library for rules of use; OA articles are governed by the applicable Creative Commons License

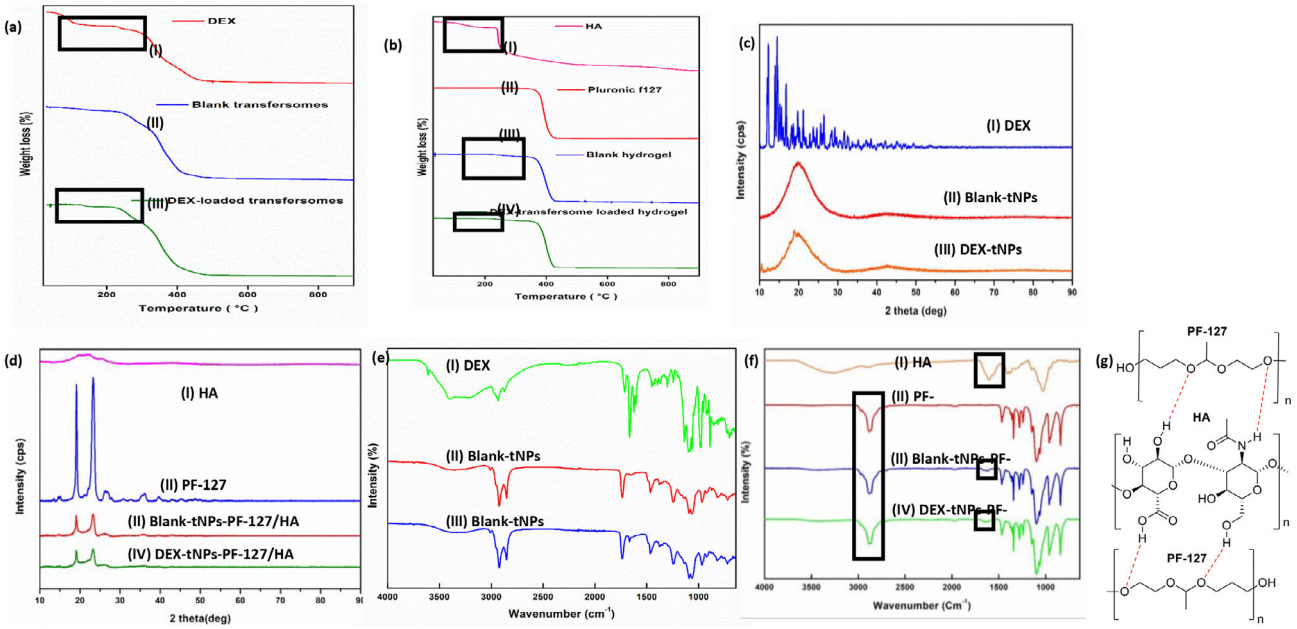

FIGURE 4 | TGA thermogram of (a) DEX (l), blank-tNPs (ll), and DEX-tNPs (lll). (b) TGA thermograms of HA (l), PF-127 (ll), tNPs-PF-127/HA hydrogel (lll), and DEX-tNPs-PF-127/HA hydrogel (lV). (c) XRD diffractograms of DEX (l), Blank-tNPs (ll), and DEX-tNPs (lll). (d) XRD diffractograms of HA (l), PF-127 (ll), tNPs-PF-127/HA hydrogel (lll), and DEX-tNPs-PF-127/HA hydrogel (lV). (e) FTIR spectra of DEX (l), Blank-tNPs (ll), and DEX-tNPs (lll). (f) HA (l), PF-127 (ll), tNPs-PF-127/HA hydrogel (lll), and DEX-tNPs-PF127/HA hydrogel (lV) and (g) the proposed molecular interactions between PF-127 and HA.

in PDI. No sedimentation or turbidity changes were observed in tNPs stored at 4°C and 25°C, indicating stable formulations (Table S4).

3.6 | In Vitro DEX Release Profiles From tNPs and tNPs-PF-127/HA Hydrogel

Cumulative drug release at pH 7.4 showed free DEX fully released in 10 h (Figure 5a (l)), while the DEX-loaded tNPs had a sustained release of DEX, with 60% released in 10 h and 90% of the drug released over 72 h (Figure 5a (ll)). In HA/P127 hydrogel, DEX had a burst release (62.5%) in the first week, followed by sustained release for up to 7 weeks (Figure 5b). The knee simulator showed 48% release in 30 min, then sustained release for 3.5 h (Figure 5c), aligning with reported 12–15-day durations for similar formulations [32, 33].

3.7 | Rheological Characterization and Syringeability of DEX-tNPs-PF127/HA Hydrogels

Dynamic rheological analysis of the DEX-tNPs-PF-127/HA hydrogel showed gelation at 30°C, with viscosity rising from 1627.83 mPa at room temperature to 9295.78 mPa at 37°C (Figure 6a). The stress sweep identified the LVE region plateauing at 9175 Pa (Figure 6b), while the frequency sweep confirmed structural stability post-administration (G' exceeding G'' with a crossover point at higher frequencies), thus ensuring sustained drug release (Figure 6c). The yield stress was 108.8 Pa, (Figure 6d), and thixotropy tests showed a hysteresis loop (38 170 Pa), indicating thixotropic behavior (Figure 6e). The hydrogel transitioned to a gel within 150 s at 37°C. Syringeability testing showed a maximum extrusion force of 24 N using a 22-gauge needle (Figure 6f). The thermoresponsive behavior of the hydrogel formulations was visually confirmed using the vial inversion method, as shown in Figure 6g. At 4°C, both the blank and DEX-tNPs-loaded PF-127/HA hydrogels remained in a free-flowing sol state, easily flowing upon inversion of the vials. However, when the temperature was raised to 37°C, a clear sol-to-gel transition was observed, with the formulations forming stable gels that retained their shape (Figure 6g).

3.8 | Cytocompatibility Studies and IL-4 Quantification From RAW 264.7 Macrophage Cells After Treatment

Microphotographs showed RAW 264.7 macrophages transitioning from an elongated (Figure 7a) to a circular morphology post-treatment (Figure 7b). The MTT assay confirmed cell viability above 70% for all treatments, with Blank-tNPs hydrogel exhibiting the highest viability (107.14%), Figure 7c. IL-4 secretion analysis used to evaluate anti-inflammatory effects indicated that the Blank-tNPs hydrogel had the highest IL-4 levels (135.5 pg/mL), followed by the Blank-tNPs (107.85 pg/mL) and the DEX-tNPs hydrogel (107 pg/mL). The DEX-loaded tNPs (63.37 pg/mL) and DEX alone (78.27 pg/mL) showed a lower IL-4 secretion, while the negative control had undetectable IL-4 levels (−38.55 pg/mL), confirming no IL-4 production (Figure 7d).

4 | Discussion

A DEX-tNPs-PF-127/HA hydrogel was developed for IA delivery in OA, with the optimized formulation analyzed for morphology,

26884011, 2025, 12, Downloaded from https://onlinelibrary.wiley.com/doi/10.1002/nano.70047 by University Of Witwatersrand, Wiley Online Library on [15/12/2025]. See the Terms and Conditions (https://onlinelibrary.wiley.com/terms-and-conditions) on Wiley Online Library for rules of use; OA articles are governed by the applicable Creative Commons License

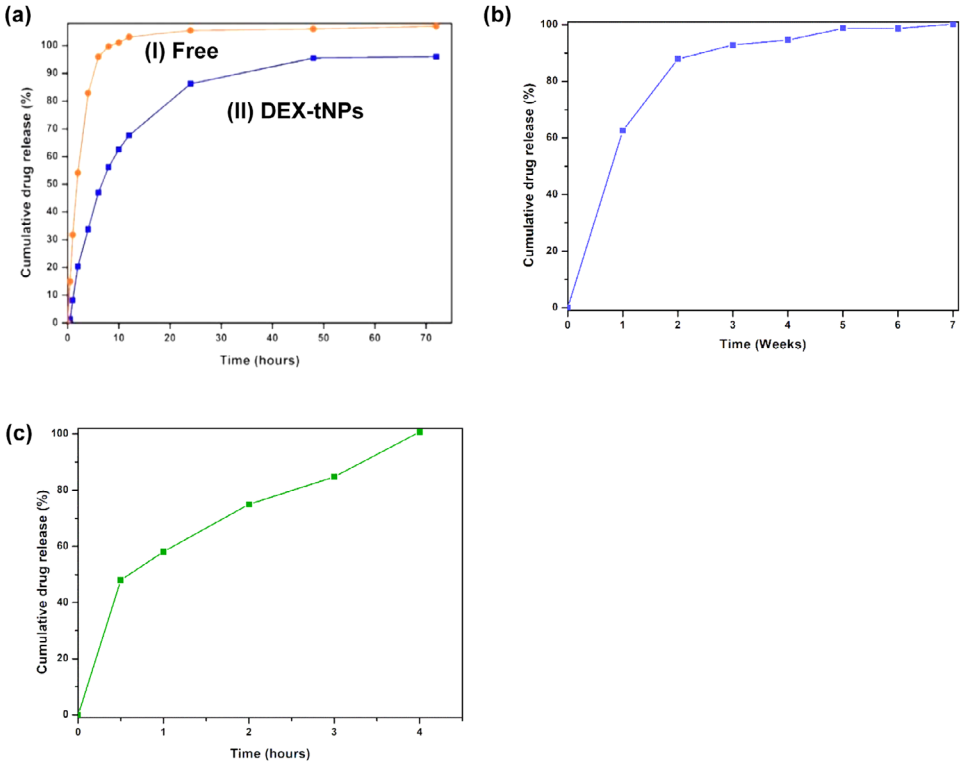

FIGURE 5 | DEX-release profiles from (I) free drug (II) DEX-tNPs, (b) tNPs-PF-127/HA hydrogel at pH 7.4, and (c) tNPs-PF-127/HA obtained using the knee joint simulator.

physicochemical properties, stability, and in vitro DEX release. Computational modeling predicted successful DEX loading at the tNP centroid, with phosphatidylcholine ensuring controlled release via nonpolar interactions and hydrogen bonding. Phosphatidylcholine was selected for its vesicle-forming ability, safety, and cost-effectiveness. Edge activators enhanced flexibility and permeability, DDAB stabilized surface charge, and cholesterol reinforced the bilayer. These findings supported tNP synthesis for optimized nanoparticle formulation and controlled drug delivery.

tNPs were synthesized via thin layer film hydration, with SEM and TEM confirming their nanosized, and spherical morphology. DLS showed a size increase from 60.93 to 76.43 nm upon DEX loading, with a lower PDI (0.183) compared to the blank tNPs (0.191) suggesting a stabilizing effect, reducing aggregation, and indicative of a highly monodispersed sample (PDI < 0.5). The zeta potential decreased to 10.58 mV, confirming drug entrapment. A high encapsulation efficiency (~98%), maintaining a cationic charge and flexibility of the tNPs supported adaptability to narrow joint spaces, enhancing drug penetration. These findings highlight the tNPs as a stable, and efficient drug delivery system for OA treatment with potentially improved tissue permeability.

The DEX-loaded tNPs were successfully incorporated into the PF-127/HA hydrogel, reducing pore size and enabling controlled drug release via hydrogel degradation. SEM (Figure 3a,b) confirmed a porous structure, facilitating sustained release, with degradation acting as a rate-limiting step for prolonged therapeutic effects.

The thermogram confirmed DEX presence in the tNPs with initial degradation at 120°C, while major decomposition occurred after 350°C due to phosphatidylcholine breakdown. Hydrogel incorporation improved stability up to 380°C, further supporting successful drug encapsulation and aligning with the literature findings [34–36].

XRD confirmed pure DEX as crystalline (by presence of sharp and intense peaks), while the blank and DEX-loaded tNPs were amorphous (displaying diffraction peaks [2θ] at 20° and 40°), indicating successful encapsulation (Figure 4c). Stability studies favored 4°C storage, with no color change or phase separation over 3 months. PF-127 was crystalline, HA was amorphous, and their hydrogels exhibited unchanged diffractograms, supporting successful drug loading. The reduced crystallinity of PF-127 in the hydrogel systems was attributed to amorphous HA. Hydrogen bonding influenced diffractogram peak intensity, reducing crystallinity and increasing structural disorder, as shown in Figure 4d–g [37, 38].

FTIR analysis confirmed the presence of key functional groups in both the blank and DEX-loaded tNPs, with broadband at 3375.35 cm^{-1} indicating hydroxyl groups from cholesterol and phosphatidylcholine. Peaks at 2923.14 and 2853.47 cm^{-1} corresponded to CH_2 stretching vibrations, while the 1736.88 cm^{-1} band indicated C═O stretching from phosphatidylcholine. No DEX-specific bands were observed, confirming successful encapsulation without unwanted interactions (Figure 4e). FTIR spectra of the DEX-loaded and blank-tNPs hydrogels showed characteristic bands of PF-127 and HA, confirming their incorporation into the hydrogel matrix and validating the formulation's compatibility and stability. The absence of the bands of the tNPs and pure DEX (Figure 4f)

26884011, 2025, 12, Downloaded from https://onlinelibrary.wiley.com/doi/10.1002/nano.70047 by University Of Witwatersrand, Wiley Online Library on [15/12/2025]. See the Terms and Conditions (https://onlinelibrary.wiley.com/terms-and-conditions) on Wiley Online Library for rules of use; OA articles are governed by the applicable Creative Commons License

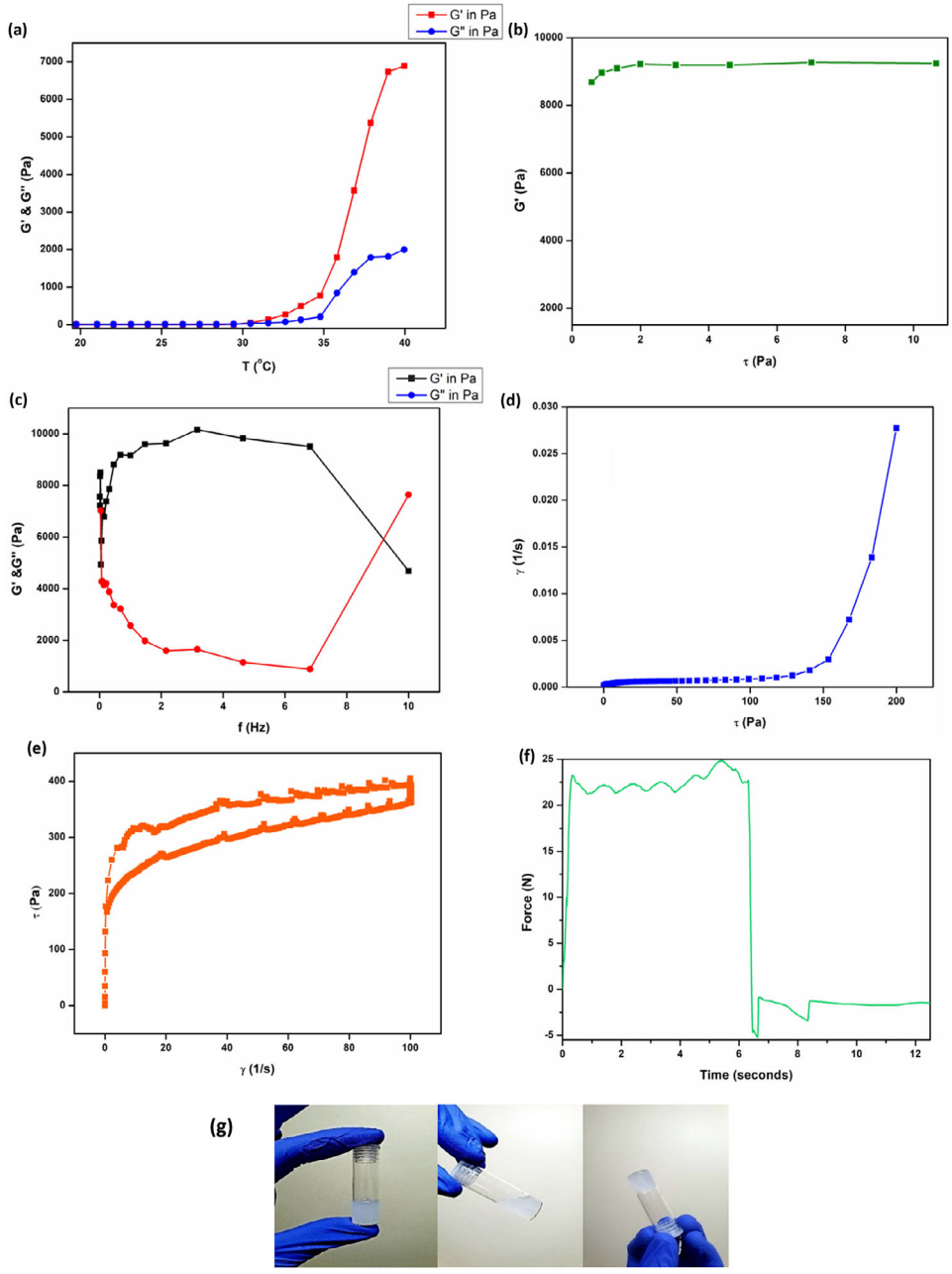

FIGURE 6 | Rheograms presenting the (a) temperature ramp, (b) stress sweep, (c) frequency sweep, (d) yield stress, (e) thixotropy, (f) syringeability profile of tNPs-PF-127/HA, and photographic images of inverted vials demonstrating the thermosensitive sol–gel transition of the hydrogel formulations (g).

proved that the particles were embedded into the hydrogel matrices.

The dialysis method showed sustained DEX release from the tNPs over 72 h versus 10 h for free drug at pH 7.4. The hydrogel extended release to over 6 weeks using the dialysis method, while a knee simulator estimated complete in vivo release in 6 days in normal (non-arthritic) movements. The two release methods suggest that administration of patient treatment may range from once a week to only 4–6 IA injections annually. Both these methods show that this drug delivery system could reduce drug administration frequency in OA, improving patient compliance. The marked discrepancy between the drug release profiles obtained using the dialysis method and the knee joint simulator is attributable to differences in environmental complexity and physiological relevance. Dialysis-based release systems provide a static and idealized release condition, where the hydrogel is exposed to an excess of release medium with no mechanical interference. In contrast, the knee joint simulator recreates IA conditions that are critical factors influencing gel integrity, drug diffusion, and NPs behavior. As a result, drug release in the joint simulator is significantly slower and more sustained, aligning better with the expected in vivo performance of the smart delivery system [39].

Figure 4a shows $G'' > G'$, indicating that the DEX-tNP-PF127/HA hydrogel was a solution at lower temperatures, transitioning

26884011, 2025, 12, Downloaded from https://onlinelibrary.wiley.com/doi/10.1002/nano.70047 by University Of Witwatersrand, Wiley Online Library on [15/12/2025]. See the Terms and Conditions (https://onlinelibrary.wiley.com/terms-and-conditions) on Wiley Online Library for rules of use; OA articles are governed by the applicable Creative Commons License

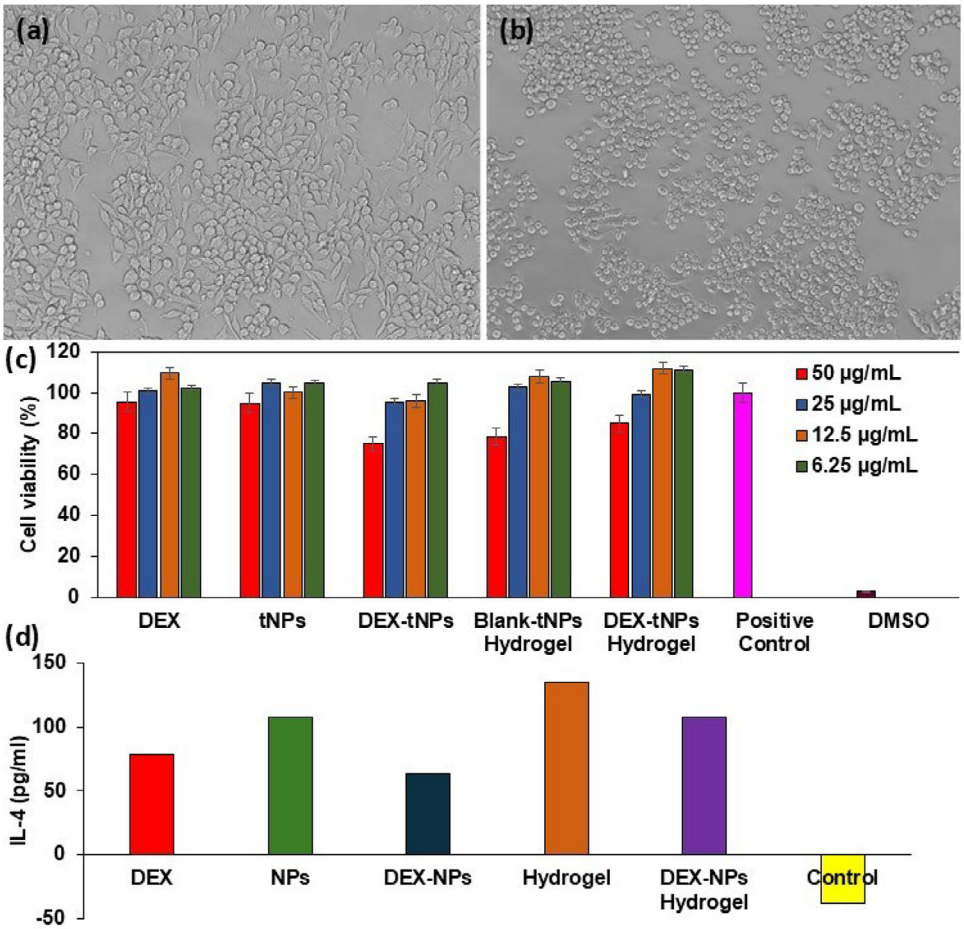

FIGURE 7 | (a) Micrographs of 264.7 RAW macrophage cells before treatment at 20× for (b) 264.7 RAW macrophage cells post 72 h of treatment at 20× (scale: 1 cm = 100 µm). (c) Cell proliferation and viability of murine RAW 264.7 macrophages exposed to DEX, Blank-tNPs, DEX-tNPs, Blank-tNPs hydrogel, and DEX-tNPs hydrogel composites for 72 h. (d) Quantification of IL-4 secretion by Raw Macrophages post-treatment with various formulations (25 µg/ML) after 24 h of incubation (Control: Blank/negative control).

to a gel at 30°C. The crossover point ($G' = G''$) marked a balance between storage and loss modulus. The LVE region was identified at 9175 Pa, suggesting that the hydrogel network could withstand up to 100 Pa stress before deformation. At 37°C, $G' > G''$, confirming gel-like behavior at body temperature, which is ideal for the desired application. The hydrogel's 108 Pa yield stress ensured easy IA injection, adaptation to joint contours, and showed enhanced stability and robustness [40]. Shear-thinning properties supported self-healing, syringeability, and structural recovery post-injection, enhancing its suitability for OA treatment.

The DEX-tNPs-PF-127/HA hydrogel required a maximum force of 24 N to be expelled from a 22-gauge needle syringe (Figure 5f). Although higher than the ones in similar studies, the extrusion force is in the acceptable range [41]. This force is suitable for IA injections since 30 N is generally considered the maximum force for a manual injection [42]. The 150-s gelation period ensures ease of handling and rapid sol–gel transition post-injection.

The MTT assay confirmed all treatments were non-toxic to RAW 264.7 cells (Figure 7c). The Blank-tNPs and DEX-tNPs hydrogel slightly reduced viability at 50 µg/mL, while the blank tNPs-PF-127/HA hydrogels and DEX-tNPs-PF-127/HA hydrogels consistently enhanced cell viability, suggesting a possible protective or proliferative effect. The results illustrated the non-toxic nature of the formulation, which is encouraging for potential clinical translation.

The study evaluated IL-4 secretion from RAW 264.7 macrophages to assess anti-inflammatory effects in OA [43]. All treatments increased IL-4, with Blank-tNPs hydrogel inducing the highest secretion (135.51 pg/mL), likely due to high-molecular-weight HA promoting M2 macrophage polarization [44, 45]. Surprisingly, compared to the Blank-tNPs, the DEX-tNPs, and DEX-tNPs loaded hydrogel elicited lower IL-4, suggesting encapsulation attenuated DEX's effect. DEX is known to inhibit the secretion of multiple cytokines, including IL-4 and IL-13, both of which are key mediators of M2 macrophage polarization and anti-inflammatory responses. This suppression may occur through interference with the JAK/STAT6 signaling pathway, which is activated downstream of IL-4 and regulates the transcription of associated anti-inflammatory genes [46]. Morphological analysis confirmed M1-to-M2 macrophage transition (Figure 7a,b), supporting cytokine-driven anti-inflammatory activity.

While inflammation is indeed a multifactorial and complex process involving numerous signaling pathways, our results

26884011, 2025, 12, Downloaded from https://onlinelibrary.wiley.com/doi/10.1002/nano.70047 by University Of Witwatersrand, Wiley Online Library on [15/12/2025]. See the Terms and Conditions (https://onlinelibrary.wiley.com/terms-and-conditions) on Wiley Online Library for rules of use; OA articles are governed by the applicable Creative Commons License

indicate that the observed upregulation of IL-4 and the associated macrophage polarization suggest a promising immunomodulatory mechanism consistent with anti-inflammatory activity, for the Blank-tNPs and the Blank tNPs-PF-127/HA hydrogel, irrespective of DEX encapsulation.

5 | Conclusions and Limitations of the Study

5.1 | Conclusions

This study successfully developed and characterized a dexamethasone (DEX)-loaded transfersome-based hydrogel (DEX-tNPs-PF-127/HA) for intra-articular (IA) delivery in osteoarthritis (OA) treatment. The formulation demonstrated favorable physicochemical properties, including nanoscale particle size (~76 nm), a high encapsulation efficiency (98%), and shear-thinning behavior, facilitating ease of injection. Sustained drug release was achieved for up to 6 weeks, reducing the need for frequent IA injections. Biocompatibility studies confirmed that all treatments maintained cell viability above 70%, with the Blank-tNPs hydrogel showing the highest immunomodulatory effect response, likely due to high molecular weight HA promoting M2 macrophage polarization. Interestingly, encapsulated DEX exhibited slightly reduced IL-4 secretion compared to its free form, suggesting that its immunomodulatory effect response might be altered by the nanocarrier in the system. Morphological analysis confirmed M1-to-M2 macrophage transition, reinforcing the therapeutic potential of the formulation. These findings suggest that the developed hydrogel is a promising candidate for OA treatment, offering prolonged drug retention and enhanced therapeutic outcomes.

5.2 | Limitations

Despite the promising results, the study has some limitations. First, the in vitro release studies may not fully replicate the complex physiological environment of the human knee joint. Although the knee simulator provided more physiologically relevant data, in vivo animal model validation is necessary to confirm the formulation's efficacy and safety. Additionally, while IL-4 quantification indicated an immunodulatory response, a broader cytokine panel analysis could provide a more comprehensive understanding of the formulation's immunomodulatory effects. Further in vivo studies are warranted to optimize the formulation for clinical translation.

Acknowledgments

A.M. conveys special thanks to the University of the Witwatersrand's Wits Advanced Drug Delivery Platform for the opportunity to conduct this research.

Conflicts of Interest

The authors declare no conflicts of interest.

Data Availability Statement

Data is available on request.

References

1. J. D. Steinmetz, G. T. Culbreth, L. M. Haile, et al., "Global, Regional, and National Burden of Osteoarthritis, 1990–2020 and Projections to 2050: A Systematic Analysis for the Global Burden of Disease Study 2021," *Lancet Rheumatology* 5 (2023): e508–e522.

2. O. O'Sullivan, "Osteoarthritis: Pathophysiology and Classification of a Common Disabling Condition," *The Palgrave Encyclopedia of Disability* (Springer Nature Switzerland, 2024): 1–11.

3. A. Boffa, G. Merli, L. Andriolo, C. Lattermann, G. M. Salzmann, and G. Filardo, "Synovial Fluid Biomarkers in Knee Osteoarthritis: A Systematic Review and Quantitative Evaluation Using BIPEDs Criteria," *Cartilage* 13, no. S1 (2021): 82S–103S.

4. L. Wang and C. He, "Nrf2-Mediated Anti-Inflammatory Polarization of Macrophages as Therapeutic Targets for Osteoarthritis," *Frontiers in Immunology* 13 (2022): 967193.

5. S. Li, P. Cao, T. Chen, and C. Ding, "Latest Insights in Disease-Modifying Osteoarthritis Drugs Development," *Therapeutic Advances in Musculoskeletal Disease* 15 (2023): 1759720×231169839.

6. R. Sohail, M. Mathew, K. K. Patel, S. A. Hasan, P. Rajan, and N. Khan, "Effects of Non-Steroidal Anti-inflammatory Drugs (NSAIDs) and Gastroprotective Nsaids on the Gastrointestinal Tract: A Narrative Review," *Cureus* 15 (2023): e37548.

7. I. A. Jones, R. Togashi, M. L. Wilson, J. D. Heckmann, and E. D. Vangsness Jr, "Intra-Articular Treatment Options for Knee Osteoarthritis," *Nature Reviews Rheumatology* 15 (2019): 77–90.

8. K. Liu, D. Zhang, W. Wang, Q. Chen, Y. Fang, and J. Lin, "Nanoparticle-Based Drug Delivery System—A Target Strategy for Osteoarthritis Treatment," *Journal of Nanomaterials* (2021), https://doi.org/10.1155/2021/4064983.

9. A. Liu, E. Ingham, J. Fisher, and X. Jin, "Development of a Pre-Clinical Experimental Simulation Model of the Natural Porcine Knee With Appropriate Ligamentous Constraints," *PLoS ONE* 14 (2019): e0216872.

10. E. Kushan, E. Senses, A. Alkan, and M. E. Güngör, "Thermoresponsive and Injectable Composite Hydrogels of Cellulose Nanocrystals and Pluronic F127," *ACS Applied Bio Materials* 4 (2021): 3507–3517.

11. W. Hu, X. Yao, Y. Li, et al., "Injectable Hydrogel With Selenium Nanoparticles Delivery for Sustained Glutathione Peroxidase Activation and Enhanced Osteoarthritis Therapeutics," *Materials Today Bio* 23 (2023): 100864.

12. Z. Zhao, P. Wang, Z. Li, et al., "Targeted Lipid Nanoparticles Distributed in Hydrogel Treat Osteoarthritis by Modulating Cholesterol Metabolism and Promoting Endogenous Cartilage Regeneration," *Journal of Nanbiotechnology* 22, no. 1 (2024): 786.

13. Q. Ding, Y. Wang, T. Wang, et al., "A Natural Polyphenolic Nanoparticle–Knotted Hydrogel Scavenger for Osteoarthritis Therapy," *Bioactive Materials* 43 (2025): 550–563.

14. J. García-Couce, M. Tomás, G. Fuentes, I. Que, A. Almirall, and L. J. Cruz, "Chitosan/Pluronic F127 Thermosensitive Hydrogel as an Injectable Dexamethasone Delivery Carrier," *Gels* 8, no. 1 (2022): 44.

15. T. Zhao, Z. Wei, W. Zhu, M. Wang, and Y. Zhou, "Recent Developments and Current Applications of Hydrogels in Osteoarthritis," *Bioengineering* 9 (2022): 132.

16. S. Jahanbekam, N. Mozafari, A. Bagheri-Alamooti, et al., "Ultrasound-Responsive Hyaluronic Acid Hydrogel of Hydrocortisone to Treat Osteoarthritis," *International Journal of Biological Macromolecules* 240 (2023): 124449.

17. D. Rybak, J. Du, P. Nakielski, et al., "NIR-Light Activable 3D Printed Platform Nanoarchitectured With Electrospun Plasmonic Filaments for on Demand Treatment of Infected Wounds," *Advanced Healthcare Materials* 14, no. 6 (2025): 2404274.

18. T. A. Rants'o, C. J. Van der Westhuizen, R. L. van Zyl, and Y. E. Choonara, "Optimization of Covalent Docking for Organophosphates

26884011, 2025, 12, Downloaded from https://onlinelibrary.wiley.com/doi/10.1002/nano.70047 by University Of Witwatersrand, Wiley Online Library on [15/12/2025]. See the Terms and Conditions (https://onlinelibrary.wiley.com/terms-and-conditions) on Wiley Online Library for rules of use; OA articles are governed by the applicable Creative Commons License

Interaction With Anopheles Acetylcholinesterase," *Journal of Molecular Graphics and Modelling* 110 (2022): 108054.

19. M. Govender, T. A. Rants'o, Y. E. Choonara, P. Kumar, and V. Pillay, "A Micro-In-Macro Gastroretentive System for the Delivery of Narrow-Absorption Window Drugs," *Polymers* 15 (2023): 1385.

20. F. Lolicato, J. Akola, H. Martinez-Seara, M. Karttunen, and I. Vattulainen, "Nanoparticle Builder: New Software for Preparing Nanoparticles for Molecular Dynamics Simulations," *European Biophysics Journal* 46 (2017): S222–S222.

21. T. E. Gartner, III and A. Jayaraman, "Modeling and Simulations of Polymers: A Roadmap," *Macromolecules* 52 (2019): 755–786.

22. Y. Thabet, M. Elsabahy, N. G. Eissa, and M. E. M. El-Massry, "Methods for Preparation of Niosomes: A Focus on Thin-film Hydration Method," *Methods (San Diego, Calif.)* 199 (2022): 9–15.

23. H. M. Tawfeek, A. A. Abdellatif, J. A. Abdel-Aleem, and R. M. Mohyeldin, "Transfersomal Gel Nanocarriers for Enhancement the Permeation of Lornoxicam," *Journal of Drug Delivery Science and Technology* 56 (2020): 101540.

24. B. C. Garms, H. Poli, D. Baggley, and A. Petermann, "Evaluating the Effect of Synthesis, Isolation, and Characterisation Variables on Reported Particle Size and Dispersity of Drug Loaded PLGA Nanoparticles," *Materials Advances* 2 (2021): 5657–5671.

25. D. Nowak and E. Jakubczyk, "The Freeze-Drying of Foods—The Characteristic of the Process Course and the Effect of Its Parameters on the Physical Properties of Food Materials," *Foods* 9 (2020): 1488.

26. N. Saadatkhah, A. C. Garcia, S. Ackermann, and G. Wegner, "Experimental Methods in Chemical Engineering: Thermogravimetric Analysis—TGA," *Canadian Journal of Chemical Engineering* 98 (2020): 34–43.

27. C. A. Omolo, N. A. Megrab, R. S. Kalhapure, and Y. E. Choonara, "Liposomes With pH Responsive 'On and off' switches for Targeted and Intracellular Delivery of Antibiotics," *Journal of Liposome Research* 31 (2021): 45–63.

28. I. R. Schmolka, "Artificial Skin I. Preparation and Properties of Pluronic F-127 Gels for Treatment of Burns," *Journal of Biomedial Materials Research* 6 (1972): 571–582.

29. H. Y. Hsieh, W. Y. Lin, A. L. Lee, and K. Y. Chen, "Hyaluronic Acid on the Urokinase Sustained Release With a Hydrogel System Composed of Poloxamer 407: HA/P407 Hydrogel System for Drug Delivery," *PLoS ONE* 15 (2020): e0227784.

30. P. Panyamao, W. Ruksiriwanich, P. Sirisa-Ard, and N. Saito, "Injectable Thermosensitive Chitosan/Pullulan-Based Hydrogels With Improved Mechanical Properties and Swelling Capacity," *Polymers* 12 (2020): 2514.

31. J. Giliomee, L. C. du Toit, P. Kumar, and Y. E. Choonara, "Evaluation of Composition Effects on the Physicochemical and Biological Properties of Polypeptide-Based Hydrogels for Potential Application in Wound Healing," *Polymers* 13 (2021): 1828.

32. M. Al-Sibani, A. Al-Harrasi, R. H. H. Neubert, and M. Müller, "Characterization of Linear and Chemically Cross-Linked Hyaluronic Acid using Various Analytical Techniques Including FTIR, ESI-MS, H1 NMR, and SEM," *Journal of Biochemistry and Analytical Studies* 3 (2018): 1–8.

33. B. J. Cole and H. R. Schumacher, "Injectable Corticosteroids in Modern Practice," *Journal of the American Academy of Orthopaedic Surgeons* 13 (2005): 37–46.

34. V. H. Mouser, F. P. Melchels, J. Visser, P. J. Dijkstra, and J. Malda, "Yield Stress Determines Bioprintability of Hydrogels Based on Gelatin-Methacryloyl and Gellan Gum for Cartilage Bioprinting," *Biofabrication* 8 (2016): 035003.

35. G. L. Pérez-González, L. J. Villarreal-Gómez, A. Olivas-Sarabia, and J. L. García-García, "Development, Characterization, and In Vitro Assessment of Multilayer Mucoadhesive System Containing Dexamethasone Sodium Phosphate," *International Journal of Polymeric Materials and Polymeric Biomaterials* 70 (2021): 1316–1328.

36. P. Kumar, S. K. Singh, V. Handa, and K. Thakur, "Oleic Acid Nanovesicles of Minoxidil for Enhanced Follicular Delivery," *Medicines* 5 (2018): 103.

37. D. T. Nguyen, V. T. Dinh, L. H. Dang, and P. H. Tran, "Dual Interactions of Amphiphilic Gelatin Copolymer and Nanocurcumin Improving the Delivery Efficiency of the Nanogels," *Polymers* 11 (2019): 814.

38. A. Karava, M. Lazaridou, S. Nanaki, and D. G. Fatouros, "Chitosan Derivatives With Mucoadhesive and Antimicrobial Properties for Simultaneous Nanoencapsulation and Extended Ocular Release Formulations of Dexamethasone and Chloramphenicol Drugs," *Pharmaceutics* 12 (2020): 594.

39. M. Yu, W. Yuan, D. Li, A. Schwendeman, and S. P. Schwendeman, "Predicting Drug Release Kinetics From Nanocarriers Inside Dialysis Bags," *Journal of Controlled Release* 315 (2019): 23–30.

40. N. Islam, M. Irfan, A. F. Zahoor, and S. Khan, "Improved Bioavailability of Ebastine Through Development of Transfersomal Oral Films," *Pharmaceutics* 13 (2021): 1315.

41. D. Rybak, C. Rinoldi, P. Nakielski, et al., "Injectable and Self-Healable Nano-Architectured Hydrogel for NIR-Light Responsive Chemo- and Photothermal Bacterial Eradication," *Journal of Materials Chemistry B* 12, no. 7 (2024): 1905–1925.

42. N. El Kechai, A. Bochot, N. Huang, and M. Fattal, "Effect of Liposomes on Rheological and Syringeability Properties of Hyaluronic Acid Hydrogels Intended for Local Injection of Drugs," *International Journal of Pharmaceutics* 487 (2015): 187–196.

43. X. Zou, H. Xu, and W. Qian, "Macrophage Polarization in the Osteoarthritis Pathogenesis and Treatment," *Orthopaedic Surgery* 17, no. 1 (2025): 22–35.

44. P. Wojdasiewicz, Ł. A. Poniatowski, and D. Szukiewicz, "The Role of Inflammatory and Anti-Inflammatory Cytokines in the Pathogenesis of Osteoarthritis," *Mediators of Inflammation* 2014 (2014): 561459.

45. M. A. Shahbazi, M. Sedighi, T. Bauleth-Ramos, R. Shahbazi, and H. Santos, "Targeted Reinforcement of Macrophage Reprogramming Toward M2 Polarization by IL-4-Loaded Hyaluronic Acid Particles," *ACS Omega* 3 (2018): 18444–18455.

46. L. Jiang, S. Gao, L. Qiu, L. Zhu, Y. Li, and R. Jin, "Impact of Dexamethasone on Expression of ORMDL3 and STAT6 in Murine Models of Asthma," *Iranian Journal of Pediatrics* 4 (2017): e9334.

Supporting Information

Additional supporting information can be found online in the Supporting Information section.

Supporting file 1: nano70047-sup-0001-SuppMat.docx.

26884011, 2025, 12, Downloaded from https://onlinelibrary.wiley.com/doi/10.1002/nano.70047 by University Of Witwatersrand, Wiley Online Library on [15/12/2025]. See the Terms and Conditions (https://onlinelibrary.wiley.com/terms-and-conditions) on Wiley Online Library for rules of use; OA articles are governed by the applicable Creative Commons License